

Liquid–solid-like transition in quasi-one-dimensional driven granular media

M. G. CLERC¹, P. CORDERO¹, J. DUNSTAN¹, K. HUFF^{1*}, N. MUJICA^{1†}, D. RISSO² AND G. VARAS¹

¹Departamento de Física, CIMAT, Facultad de Ciencias Físicas y Matemáticas Universidad de Chile, Avenida Blanco Encalada 2008, Santiago, Chile

²Departamento de Física, CIMAT, Facultad de Ciencias, Universidad del Bío-Bío, Avenida Collao 1202, Concepción, Chile

*Present address: Department of Physics, James Franck Institute, The University of Chicago, 5640 S. Ellis Avenue, Chicago, Illinois 60637, USA

†e-mail: nmujica@dfi.uchile.cl

The theory of non-ideal gases at thermodynamic equilibrium, for instance the van der Waals gas model, has played a central role in our understanding of coexisting phases, as well as the transitions between them. In contrast, the theory fails with granular matter because collisions between the grains dissipate energy, and their macroscopic size renders thermal fluctuations negligible. When a mass of grains is subjected to mechanical vibration, it can make a transition to a fluid state. In this state, granular matter exhibits patterns and instabilities that resemble those of molecular fluids. Here, we report a granular solid–liquid phase transition in a vibrating granular monolayer. Unexpectedly, the transition is mediated by waves and is triggered by a negative compressibility, as for van der Waals phase coexistence, although the system does not satisfy the hypotheses used to understand atomic systems. The dynamic behaviour that we observe—coalescence, coagulation and wave propagation—is common to a wide class of phase transitions. We have combined experimental, numerical and theoretical studies to build a theoretical framework for this transition.

In the course of recent decades, much effort has been devoted to study the phases exhibited by granular matter. However, the richness and complexity of the static and dynamic behaviour of granular materials still present a major challenge in physics^{1,2}. Fluidized granular matter exhibits a variety of phenomena that resemble those of molecular fluids: patterns and instabilities, such as Faraday instability^{3,4} and Rayleigh–Benard-type convection⁵. Depending on the forcing parameters, vertically vibrated granular layers present different patterns such as stripes, squares, hexagons, spirals, interfaces and oscillons^{6–8}. In fact, it has been shown that these subharmonic standing-wave patterns appear when the system has undergone a solid-to-liquid-like transition⁹.

Recently, several granular systems that undergo interesting phase transitions have been reported^{10–17}. Two of these systems are relevant to the present work. The first one is an experimental and molecular dynamic simulation study of quasi-two-dimensional (2D) systems consisting of submonolayers of grains subjected to vertical vibration. This system shows a liquid–solid-like phase transition, with a coexistence regime characterized by a dense cluster of closely packed, almost immobile grains (crystal structure) surrounded by a fluid of agitated particles^{14,15}. Here, it is argued that the phase behaviour can be understood through entropy maximization in analogy to equilibrium hard-sphere systems¹⁸. However, dramatic non-equilibrium effects are present, including a significant difference in the granular temperatures of the two phases. We underline that this type of behaviour—far from equilibrium—can be expected if the phase transition is led by a non-equilibrium potential¹⁹.

The second system is a fluidized granular layer in two spatial dimensions, which exhibits a gas–liquid-like phase separation^{16,17}, analogous to the spinodal decomposition of the gas–liquid

transition in the van der Waals model²⁰. At the onset of this phase transition, the system reveals rich dynamic behaviour characterized by the appearance, coalescence and disappearance of clusters. The mechanism of this phase separation is triggered by a negative compressibility, implied by the fact that the pressure is a decreasing function of density.

The granular systems described above—microscopically well modelled by either inelastic hard- or soft-sphere approximations with no cohesive force and the associated simulations—are known to show clustering, namely, coexistence of higher- and lower-density regions. However, understanding the existence of different granular phases requires a macroscopic viewpoint. A continuous or macroscopic description of granular flows, a ‘granular hydrodynamics’, remains an open question. Here, none of this is necessary because the use of order parameter equations based on symmetry arguments is powerful enough to study the dynamics of coexistence of different phases in out-of-equilibrium granular matter^{2,21}.

Here, we report a combined experimental, numerical and theoretical study of a liquid–solid-like phase transition that takes place in a vertically vibrated fluidized dense granular system of N hard spheres confined on a horizontal plate with a top lid at height h , which is less than two particle diameters. Two experimental set-ups are considered. The first one is a long, narrow channel, with a width of the order of a few particle diameters; hence, the dynamics is quasi-1D (Fig. 1). We have considered this configuration to characterize the dynamic behaviour of the phase transition, avoiding 2D effects, such as curvature between phases or crystal orientation interaction dependence. The second set-up is used to measure the pressure as a function of particle density to clarify the physical mechanism behind this phase transition. In

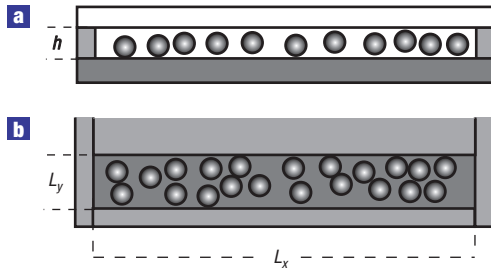


Figure 1 Schematic representation of the system. **a,b**, Side (**a**) and top (**b**) views of the system. In both experiments and molecular dynamic simulations, the cell geometry is: height $h = 1.8d$, where d is the particle diameter, length L_x and width L_y , with $L_x \gg d$ and $L_y \gtrsim d$. For the experimental pressure measurements, the geometry is $h = 1.7d$ and $L_x \sim L_y$.

molecular dynamics, we have studied both 3D systems of hard spheres and 2D systems of hard discs with gravity. Collisions are inelastic, and both static and dynamic friction coefficients are considered, as well as normal and tangential restitution coefficients. For the 3D systems, these parameters are chosen close to the experimental ones. Energy is injected by vibrating the cell as in the experiment. We underline that these simulational studies are complementary to experiments. Hence, molecular dynamics enables us to explore and characterize more quantitatively the phenomena involved in the solid–liquid transition. For example, with molecular dynamics we can examine the frictionless limit, where we observe the same type of phenomena, as well as the neighbourhood of the critical point which is a much more difficult task from an experimental point of view.

EXPERIMENTAL AND SIMULATED RESULTS

At the transition, one or more clusters appear. These clusters then undergo a coarsening process, and eventually only one single solid cluster prevails (Fig. 2). For fixed parameters, crystals with two symmetries are observed, square or triangular based, surrounded by a fluid phase as in the experimental observation in Fig. 2a,b. Similar configurations are observed in 3D molecular dynamics.

Note that triangular crystals are observed in spite of $h = 1.8d$ being slightly lower than the height of a tetrahedron formed by four spheres of diameter d in contact. This could seem unexpected, as well as the coexistence between them (Fig. 2b). However, in molecular dynamics, both symmetries coexisting with a fluid state have been observed at high densities, in a small region of the (ρ_o, h) space¹⁵, where $\rho_o = N/N_m$ and N_m is the maximum number of particles in a closed-packed monolayer. We have also observed (in experiments and molecular dynamics) the intermittence between different symmetries at fixed forcing and geometrical parameters, showing that these phases are in fact metastable. In addition, more exotic states are sometimes observed, such as crystals of alternating layers of triangular and square symmetry for different widths L_y . These states remain quite stable against perturbations. We then conclude that the geometrical constraint $L_y \gtrsim d$ has a strong effect on the observed solid symmetries, and thus plays a similar role as h in the quasi-2D system¹⁵.

3D molecular dynamic simulations in a quasi-1D configuration show the transition from a homogeneous fluid phase to the coexistence of a solid crystal and a lower density fluid phase (Fig. 2c). The observed phenomena present all the basic features observed experimentally: solid–fluid coexistence, different crystal

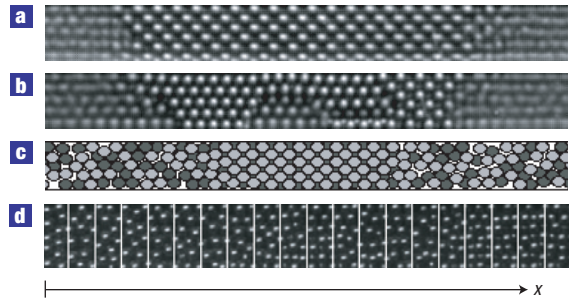


Figure 2 Solid–liquid coexistence in the confined system. **a,b**, Averaged images of typical crystal structures observed: vibration frequency $f = 65$ Hz, vibration amplitude $A = 0.29d$ and $L_y = 4.65 \pm 0.05$ mm. Different symmetries are observed: **a**, square and **b**, the coalescence of two triangular solid clusters competing with a square-symmetry cluster. **c**, Molecular dynamic 3D simulation snapshot showing a square solid cluster coexisting with a low-density fluid, with $f = 68$ Hz, $A = 0.29d$ and $L_y = 4.65d$. Light (dark) grey particles are in the upper (bottom) layer. In both experiment and molecular dynamics simulation $\rho_o = N/N_m \approx 1$, $N_m = 450$, $h = 1.8d$, $L_x = 90d$, $d = 1$ mm. **d**, Coarse-graining procedure: snapshot of the granular system in a fluid state. Vertical lines define the typical fluid elements, which are characterized by the number density $\rho(x, t)$ and the x -longitudinal momentum density $j(x, t) = \rho(v_x)$. In all images, only about half of the cell is shown for clarity.

symmetries and noise-induced transitions between them, as well as sensitivity to geometrical parameters, namely h and L_y .

As in the experimental set-up, in molecular dynamics the cell is horizontally divided into N_b bins, as in Fig. 2d, and in each bin we measure the number density ρ , the granular temperature T_g and the momentum density ρv . In the case of hard discs, we also measure the stress pressure tensor P_{ij} in each bin. In the 3D simulations, this quantity is measured at the walls. To characterize the transition, in 2D we define a contrast order parameter $c(M) = M_{\max} - M_{\min}$, where M_{\max} and M_{\min} are the extreme values of a local crystallization order parameter M , which is unity when the system is locally at its maximum density.

From 2D molecular dynamics we obtain time averages of the pressure and $c(M)$ by first letting the system relax for a given time. Figure 3a,b shows these results in the case of elastic collisions with the walls ($\epsilon_{pw} = 1$) and all friction coefficients set to $\mu_s = \mu_d = 0.05$. A constant pressure region is observed above $\rho_o \approx 1$, which is concomitant with the solid–liquid phase separation. This coexistence region shrinks when the particle–particle restitution coefficient ϵ_{pp} decreases, namely, for more inelastic collisions. Such a plateau is indeed expected once the system undergoes a transition from a homogeneous fluid state to coexisting solid and liquid states, as the negative compressibility part of the pressure–density curve is mechanically unstable and the pressure reaches a value set by the mechanical equilibrium between both phases. Notice that for the two values of ϵ_{pp} closer to unity, the pressure has a peak before entering the plateau. This is because quasi-elastic granular systems relax slowly and our measurements were not long enough to fully relax the system. Our results suggest that somewhere below $\epsilon_{pp} = 0.4$ the plateau might disappear, namely, a critical point would be reached. In the opposite limit, the system with quasi-elastic particles becomes totally fluidized, whereas if particle collisions are more dissipative, both phases are present. Hence, somewhere in between, a second critical point certainly exists. Finally, the molecular dynamics data shown in Fig. 3a reach down to $\epsilon_{pp} = 0.4$ because we had difficulties in getting reliable results for smaller values. When the system becomes too

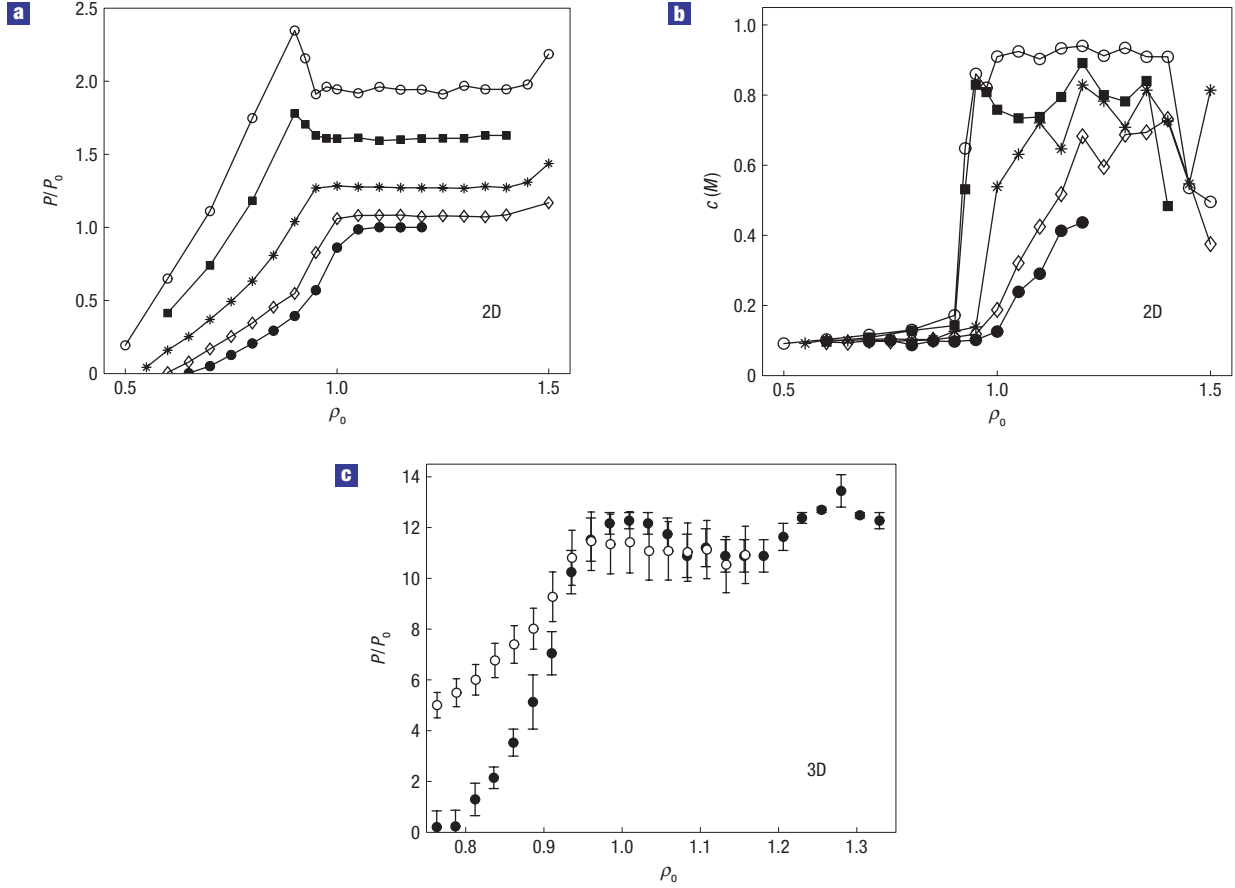


Figure 3 Pressure versus density measurements. **a,b,** Molecular dynamics pressure measurements and contrast order parameter for a confined hard-disc (2D) system. These results show that the pressure plateau is concomitant with the solid–liquid phase separation. Pressure is normalized by $P_0 = \rho_{\text{mx}} v_0^2$, where ρ_{mx} is the maximum mass density that fits in a monolayer and $v_0 = 2\pi fA$ is the vibration’s maximum velocity. Simulation parameters are $40 \leq N \leq 400$, $L_x = 400d$, $h = 1.8d$, $A = 0.35d$, $f = 10\sqrt{g/d}/\pi$, $\mu_s = \mu_d = 0.05$, $\epsilon_{pw} = 1$, $\epsilon_{pp} = 0.996$ (open circles), 0.9 (filled squares), 0.8 (asterisks), 0.6 (open diamonds) and 0.4 (filled circles), where $\mu_{s,d}$ stands for static or dynamic friction coefficients and ϵ_{pw} (ϵ_{pp}) stands for particle–particle (particle–wall) restitution coefficients. **c,** Experimental (filled circles) and molecular dynamics (open circles) results obtained in 3D shallow systems. Set-up: $d = 3$ mm, $L_x = 18.5d$, $L_y = 19d$, $h = 1.7d$, $f = 70$ Hz and $A = 0.034d$. A constant-pressure region is observed in the range $\rho_0 = 1–1.3$ for experiments, and $\rho_0 = 1–1.15$ for molecular dynamics. The experimental error bars are due to a combination of uncertainties associated with the angle measurement as well as standard deviations in other factors affecting the overall granular pressure. For the molecular dynamics results, the errors are the standard deviation from the mean.

dense and with so much dissipation, the collision rate increases and the algorithm tends to collapse.

Experimental and 3D molecular dynamics measurements of the pressure as a function of density also show such a pressure plateau, as shown in Fig. 3c. In fact, keeping all other parameters fixed, a constant pressure region is observed in the range $\rho_0 = 1–1.3$ for experiments and $\rho_0 = 1–1.15$ for molecular dynamics. Observations confirm that this plateau indeed corresponds to the coexistence region, as a square-symmetry solid crystal coexisting with a fluid state is observed solely in this region. With our current experimental set-up, reliable higher-density pressure measurements are difficult. In the numerical case, the event-driven algorithm is not suitable for high-density simulations.

MACROSCOPIC DESCRIPTION

To give a macroscopic, dimensionless description of the observed phase transition, we introduce two scalar order parameters, the number density and the longitudinal momentum density, ρ and j , respectively. Owing to the aspect ratio of the system, these order

parameters have a fast $\{y, z\}$ -dependence and a slow x -dependence. Averaging over y and z , we end up working with $\rho(x, t)$ and $j(x, t)$. This reduction is possible owing to a separation of time and space scales, which allows for a description in terms of the slowly varying macroscopic variables. These are in fact fluctuating variables, owing to the elimination of a large number of fast variables whose effect can be modelled including suitable stochastic terms in the partial differential equation that describes the system. Figure 2d shows the coarse graining grid used to obtain these average variables. Using a similar method as in refs 16,17, we have derived an equation for the slow macroscopic variables that governs the dynamics of the phase separation, even when we consider friction. The number density satisfies the damped van der Waals normal-form equation

$$\partial_{tt} u = \partial_{xx} [\epsilon u + u^3 - \partial_{xx} u + \nu \partial_t u] - \sigma \partial_t u + \sqrt{\eta} \partial_x \zeta(x, t), \quad (1)$$

where $\partial_t \rho = -\partial_x j$, $u = \rho - \rho_c$ and ρ_c is the density at the critical point (that is, the density value for which the system pressure exhibits a plateau). The control parameter ϵ is inversely proportional to the compressibility coefficient. The term

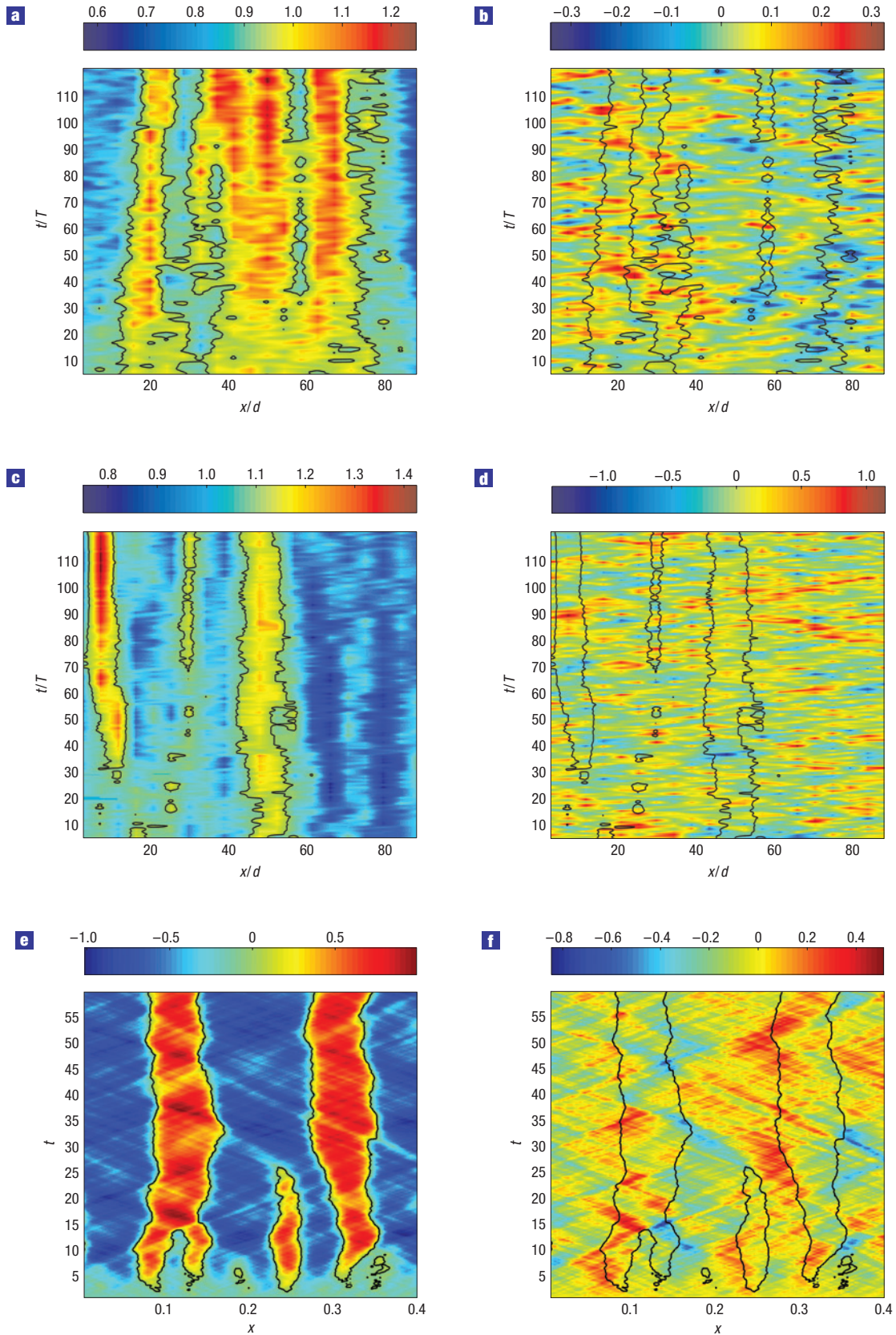


Figure 4 Density and longitudinal momentum space–time diagrams for early stages of the solid cluster formation. **a, b**, Experimental results for ρ and $\rho\langle v_x \rangle$ respectively obtained for $f = 70$ Hz, $A = 0.1d$, $L_y = 6.2$ mm, $\rho_0 \approx 1$ and $N_m = 630$. Time and space are normalized by oscillation period $T = 1/f$ and d respectively. **c, d**, Molecular dynamics simulational results for ρ and $\rho\langle v_x \rangle$ respectively, with $\rho_0 = 1$, $L_y = 6.2d$, $L_z = 1.8d$, $L_x = 90d$, $f = 70$ Hz and $A = 0.1d$. **e, f**, Results from the damping van der Waals normal form, equation (1), in the limit where noise, friction and viscosity are important, $\varepsilon = -0.5$, $u_0 = -0.155$, $\eta = 0.5$, $\nu = 1.0$ and $\sigma = 0.2$.

$\varepsilon u + u^3 = P(u)$ stands for the effective pressure close to the critical density and $\partial_{xxxx}u$ is an interface tension term, which is usually neglected in hydrodynamic fluid theory. A derivation of such a term from a granular hydrodynamic theory has been obtained from the adiabatic elimination of the granular temperature¹⁷. The term $\nu \partial_{xxx}u$ is the diffusion one, whereas $\sigma \partial_t u$ is a damping term originated by the friction with the walls. Contrary to refs 16,17, both friction (σ) and noise (η) terms are essential to describe the dynamics exhibited by the experimental and molecular dynamics results presented in this work, as explained below.

Notice that the previous model has a non-equilibrium potential¹⁹ $\mathcal{F} = \int dx \{ \varepsilon u^2 + u^4/2 + (\partial_x u)^2 \}/2$, where the last term accounts for the interface energy. Hence, the dynamics of the system close to the critical point is of the relaxation type, that is, the dynamics is characterized by the minimization of the free energy \mathcal{F} . Therefore, close to the critical point (small ε), the granular system has a dynamic behaviour similar to that of equilibrium systems.

Conservative phase transitions are characterized by diffusive dynamics. These are described by one order parameter, and are ubiquitous in nature (see ref. 22 and references therein). In particular, the electrostatically driven granular media phase transition is of the diffusive type^{12,13}. On the contrary, equation (1) is a universal model that describes a non-diffusive conservative phase transition driven by waves, and has two order parameters (u and $\partial_t u$). To our knowledge, the solid–liquid transition of a vibrating monolayer is the first experimental observation of this type of behaviour. Other experimental candidates that could exhibit this type of first-order transition are helium in a superfluid state^{23,24} and a liquid–gas-like coexisting granular monolayer^{16,17}.

The main features of model equation (1) are that it exhibits phase separation, and for small (large) damping and viscosity the transient dynamics is led by nonlinear waves (diffusive dynamics). Experimentally, quantitative results are obtained from high-speed video analysis. Figure 2d schematically shows the coarse graining procedure, where each image is divided into N_b bins, which define our fluid elements. Through particle position detection, subsequent particle tracking enables us to define, for each of these bins, the following coarse-grained quantities: horizontal granular temperature $T_g = \langle v_x^2 + v_y^2 \rangle$, number density ρ and longitudinal and transverse momenta $\rho \langle v_x \rangle$ and $\rho \langle v_y \rangle$, respectively. Here, $\rho = n/N_{mb}$, where n is the number of particles in one bin at a given time and $N_{mb} = N_m/N_b$ is the maximum number of particles in a closed-packed monolayer that fit in one bin. Finally, $\langle v_x \rangle$ and $\langle v_y \rangle$ are averaged over all particle velocities within each bin.

Representative space–time segments of the history of the system are used to show the evolution of ρ and $\rho \langle v_x \rangle$ in Fig. 4. Figure 4a,b shows experimental data, c,d shows hard-sphere molecular dynamics results and e,f shows the order parameter model results. Number-density contour lines at $\rho = 1$ are superposed on each experimental and molecular dynamics space–time diagram. For the order parameter model, contour lines represent $\rho = \rho_c$ ($u = 0$). Strong correlations are observed between number density and longitudinal momentum. In addition, correlations of both transverse momentum and granular temperature with number density are also important even though we do not show them here. Figure 4 shows that experiments, molecular dynamics and numerical simulation of model (1) show quite similar dynamic behaviour.

As a consequence of the small number of particles, internal noise is quite important. In fact, we observe noise-induced transitions between different states. The coarsening process does not have a purely diffusive signature as demonstrated by the comparison of experimental and molecular dynamics space–time diagrams with those obtained with our order parameter model (Fig. 4). In addition to noise, inertia is important in the coarsening

dynamics. Indeed, the x -momentum space–time diagrams present strong positive and negative bursts. In the experiment, these pulses propagate at a wave speed of order $5\text{--}50 \text{ cm s}^{-1}$. Owing to inelasticity and friction they do not propagate for long. At the early stages of solid cluster nucleation, these waves are roughly homogeneously distributed within the cell (Fig. 4b,d,f).

Model (1) exhibits similar dynamic behaviours to those shown by molecular dynamics and experiments. On the other hand, parameter exploration enables us to observe several phenomena such as cluster coarsening dynamics, noise-mediated cluster interactions, shock and rarefaction waves and so forth. To understand the dynamics, in the following, we present a brief description of the phase diagram. The dynamics of the model (1) is characterized by five parameters $\{\varepsilon, \nu, \sigma, \eta, u_0 = \int u(x, t) dx\}$. In the plane $\{\varepsilon, u_0\}$ there are three characteristic regions: fluid phase region ($\varepsilon > -2u_0^2$), coexistence region ($-2u_0^2 < \varepsilon < -3u_0^2$) and spinodal decomposition region ($\varepsilon > -3u_0^2$).

In the absence of noise ($\eta = 0$), the uniform fluidized states are the only stable states in the fluid region. This region is characterized by the perturbation of uniform states undergoing nonlinear damping wave propagation for small damping and viscosity. In particular, the system exhibits damped solitary waves, which become solitons in the limit $\nu = \sigma = 0$ (ref. 25). In the spinodal decomposition region, uniform fluidized states undergo a spatial instability—phase transition—followed by cluster formation. Later, neighbour clusters merge together to minimize the non-equilibrium potential. As nonlinear waves transport mass and momentum, in the inertial regime ($\{\nu, \sigma\} \ll 1$) the cluster interaction is mediated by waves, which is more efficient than diffusive coarsening. In the non-inertial regime, the system exhibits similar behaviour, that is, appearance of clusters; however, waves are damped and cluster interactions are now mediated by diffusion. In the coexistence region, depending of the initial conditions, either the uniform state is stable or two phases coexist. Experimentally, it is difficult to recognize this region because fluctuations can create or destroy clusters. The details of the dynamics exhibited by model (1) will be published elsewhere.

In general, the previous dynamic behaviour is not modified by the presence of noise. However, in the diffusive regime ($\nu \gg 1$), the coarsening exhibited by the system is completely modified by noise, because noise induces waves and waves lead to cluster interactions. In fact, both experiments and molecular dynamics are intrinsically noisy—because of the relatively small number of particles—and waves are highly damped. Therefore, the observed dynamics should correspond to this noisy diffusive regime. In this regime, model (1) with low-intensity noise could account for the coarsening dynamics exhibited by electrostatically driven granular media^{12,13}.

METHODS

EXPERIMENTAL DETAILS

Granular pressure measurements are obtained in a quasi-2D set-up, with $d = 3 \text{ mm}$, $L_x = 18.5d$, $L_y = 19d$ and $h = 1.7d$. This last value was chosen to force the solid phase to have a square symmetry, avoiding possible symmetry-dependence effects on the measured pressure. The system has stainless-steel walls and bottom base, and a static dissipative acrylic top lid. One wall is a 55.5-mm-wide, 57.6-mm-long pendulum (mass $M = 138.9 \text{ g}$). Measurements of its equilibrium angle (θ) allow force—and hence pressure—measurements through $F \approx Mg(\theta)/2$ for small angles²⁶. The number of particles was varied between 300 and 580 to obtain $\rho_0 = 0.74\text{--}1.45$.

The quasi-1D set-up consists of a 14.5-cm-long and 12.1-cm-wide stainless-steel plate, with four 1.5-mm-thick, 10-mm-wide aluminium walls. Of these, three are fixed and the fourth one is movable, allowing us to vary L_y/d continuously from 0 to 90, within ± 0.02 , although for a given run it is held constant by a set of screws. The system has a static dissipative acrylic top lid and $L_x/d = 90$, where $d = 1 \text{ mm}$ is the particle diameter. The system is shaken

sinusoidally by means of an electromechanical vibrator, with an amplitude A and frequency f . The vibration is monitored by an accelerometer and all of the set-up is illuminated by an array of halogen lamps. A high-speed camera (IDT X3, 1,045 fps, $1,280 \times 800$ pix²) allows visualization from above, and by particle position detection, subsequent particle tracking is possible²⁷. Images presented in Fig. 2a,b are obtained from an average of 100 images acquired at 30 fps. Space–time diagrams of Fig. 4a,b were computed from images acquired at 500 fps.

In all experiments, stainless-steel spheres were used, with the following dissipation parameters: $\mu_d = 0.13 \pm 0.03$, $\mu_s = 0.16 \pm 0.01$ and $\epsilon_{pp} = 0.87 \pm 0.04$ (steel–steel); $\mu_d = 0.22 \pm 0.03$, $\mu_s = 0.28 \pm 0.01$ and $\epsilon_{pw} = 0.92 \pm 0.02$ (acrylic–steel); $\mu_d = 0.21 \pm 0.04$, $\mu_s = 0.23 \pm 0.01$ and $\epsilon_{pw} = 0.56 \pm 0.02$ (aluminium–steel).

MOLECULAR DYNAMIC DETAILS

Our computer simulations are based in an event-driven algorithm for N hard discs (spheres) in two (three) dimensions. These particles have both translation and rotation degrees of freedom and all particles are alike (same radius and mass). Collisions are instantaneous and the collision rule makes use of four coefficients: normal and tangential restitution coefficients and static and dynamic friction coefficients²⁸. An entirely similar collision rule is used for particle–wall collisions introducing a second set of four coefficients.

In 2D molecular dynamics, there are horizontal periodic boundary conditions and the cell (horizontal walls) vibrates vertically. The vibrating cell does not move sinusoidally but follows a parabolic movement. The height of its base is

$$z_{\text{base}} = \begin{cases} A - \frac{16A}{T^2} \left(t - \frac{T}{4} \right)^2, & 0 \leq t < \frac{T}{2}, \\ \frac{16A}{T^2} \left(t - \frac{T}{2} \right) (t - T), & \frac{T}{2} \leq t < T, \end{cases} \quad (2)$$

where A is the amplitude, T is the period and t is the time modulus T . Owing to the parabolic movement, the acceleration has a constant absolute value, $a_{\text{cell}} = 32A/T^2 = 8A\omega^2/\pi^2$.

The crystallization order parameter M is defined as

$$M = \gamma \left| \sum_i (-1)^i \frac{z_i - h/2}{x_{i+1} - x_i} \right|,$$

where the index i in the sum refers to the particles in each bin, and x_i and z_i refer to the horizontal and vertical coordinates of each particle. The coefficient γ is chosen so that M is unity when the system is locally at its maximum density.

The pressure—the total longitudinal momentum flux—and the contrast order parameter are obtained by letting the system relax during 2,000 oscillation cycles of the cell and then accumulating data during another 2,000 cycles to finally obtain the time averages.

In the case of 3D molecular dynamics, collisions with all walls are inelastic with friction. The restitution and friction coefficients for collisions of the grains with the top horizontal wall are different from that of the other walls, as in the experiment. Lateral walls oscillate vertically at the same amplitude, frequency and in phase with the movement of the horizontal walls. To compare 3D molecular dynamics results with experiments, we use dissipation parameters very close, within experimental errors, to the experimental ones.

References

- Jaeger, H. M., Nagel, S. R. & Behringer, R. P. Granular solids, liquids, and gases. *Rev. Mod. Phys.* **68**, 1259–1273 (1996).
- Aranson, I. S. & Tsimring, L. S. Patterns and collective behavior in granular media: Theoretical concepts. *Rev. Mod. Phys.* **78**, 641–692 (2006).
- Douady, S., Fauve, S. & Laroche, C. Subharmonic instabilities and defects in a granular layer under vertical vibrations. *Europhys. Lett.* **8**, 621–627 (1989).
- Fauve, S., Douady, S. & Laroche, C. Collective behaviors of granular masses under vertical vibrations. *J. Physique* **50**, 187–191 (1989).
- Ramirez, R., Risso, D. & Cordero, P. Thermal convection in fluidized granular systems. *Phys. Rev. Lett.* **85**, 1230–1233 (2000).
- Melo, F., Umbanhowar, P. & Swinney, H. L. Transition to parametric wave patterns in a vertically oscillated granular layer. *Phys. Rev. Lett.* **72**, 172–175 (1994).
- Melo, F., Umbanhowar, P. & Swinney, H. L. Hexagons, kinks and disorder in oscillated granular layers. *Phys. Rev. Lett.* **75**, 3838–3841 (1995).
- Umbanhowar, P. B., Melo, F. & Swinney, H. L. Localized excitations in a vertically vibrated granular layer. *Nature* **382**, 793–796 (1996).
- Mujica, N. & Melo, F. Solid–liquid transition and hydrodynamic surface waves in vibrated granular layers. *Phys. Rev. Lett.* **80**, 5121–5124 (1998).
- Olafsen, J. S. & Urbach, J. S. Clustering, order, and collapse in a driven granular monolayer. *Phys. Rev. Lett.* **81**, 4369–4372 (1998).
- Cafiero, R., Luding, S. & Herrmann, H. J. Two-dimensional granular gas of inelastic spheres with multiplicative driving. *Phys. Rev. Lett.* **84**, 6014–6017 (2000).
- Aranson, I. S. *et al.* Electrostatically driven granular media: Phase transitions and coarsening. *Phys. Rev. Lett.* **84**, 3306–3309 (2000).
- Aranson, I. S., Meerson, B., Sasorov, P. V. & Vinokur, V. M. Phase separation and coarsening in electrostatically driven granular media. *Phys. Rev. Lett.* **88**, 204301 (2002).
- Prevost, A., Melby, P., Ego, D. A. & Urbach, J. S. Non-equilibrium two-phase coexistence in a confined granular layer. *Phys. Rev. E* **70**, 050301(R) (2004).
- Melby, P. *et al.* The dynamics of thin vibrated granular layers. *J. Phys. Condens. Matter* **17**, S2689–S2704 (2005).
- Argentina, M., Clerc, M. G. & Soto, R. van der Waals-like transition in fluidized granular matter. *Phys. Rev. Lett.* **89**, 044301 (2002).
- Cartes, C., Clerc, M. G. & Soto, R. van der Waals normal form for a one-dimensional hydrodynamic model. *Phys. Rev. E* **70**, 031302 (2004).
- Schmidt, M. & Lowen, H. Phase diagram of hard spheres confined between two parallel plates. *Phys. Rev. E* **55**, 7228–7241 (1997).
- Graham, R. & Tel, T. Nonequilibrium potential for coexisting attractors. *Phys. Rev. A* **33**, 1322–1337 (1986).
- Landau, L. D. & Lifschitz, D. *Statistical Physics* (Pergamon, Oxford, 1980).
- Cross, M. C. & Hohenberg, P. C. Pattern formation outside of equilibrium. *Rev. Mod. Phys.* **65**, 851–1112 (1993).
- Gutón, J. D., San Miguel, M. & Sanhi, P. S. in *Phase Transitions and Critical Phenomena* Vol. 8 (eds Domb, D. & Lewowitz, J. L.) (Academic, London, 1983).
- Josserand, C. & Rica, S. Coalescence and droplets in the subcritical nonlinear Schrödinger equation. *Phys. Rev. Lett.* **78**, 1215–1218 (1997).
- Josserand, C. *Dynamique des superfluides: Nucléation de vortex et transition de phase du premier ordre*, Thèse de Doctorat de l'Université de Paris VI (1997).
- Clerc, M. G. & Escaff, D. Solitary waves in van der Waals-like transition in fluidized granular matter. *Physica A* **371**, 33–36 (2006).
- Géminard, J.-C. & Laroche, C. Pressure measurement in two-dimensional horizontal granular gases. *Phys. Rev. E* **70**, 021301 (2004).
- Crocker, J. C. & Grier, D. G. Methods of digital video microscopy for colloidal studies. *J. Colloid Interface Sci.* **179**, 298–310 (1996).
- Risso, D., Soto, R., Godoy, S. & Cordero, P. Friction and convection in a vertically vibrated granular system. *Phys. Rev. E* **72**, 011305 (2005).

Acknowledgements

We gratefully acknowledge R. Soto and T. Witten for fruitful discussions and C. González for preliminary numerical simulations. The authors acknowledge support from CONICYT grants: FONDAPO No. 11980002, Fondecyt No. 1070958 (P.C., D.R.), Fondecyt No. 1070346 (N.M.), Anillo No. ACT 15 of Programa Bicentenario en Ciencia y Tecnología (M.G.C., J.D., K.H., N.M., G.V.). K.H. was supported through the Inter-American Materials Collaboration under DMR-0303072. Correspondence and requests for materials should be addressed to N.M.

Reprints and permission information is available online at <http://npg.nature.com/reprintsandpermissions/>